The International Journal of Advanced Manufacturing Technology
https://doi.org/10.1007/s00170-025-16929-2

ORIGINAL ARTICLE

Powder heating temperature, laser power and layer height in SLS 3D printing: impact on physical and mechanical properties of polyamide 12 parts

Fatima-Ezzahrae Jabri[1] · Aissa Ouballouch[2] · Mohamed Nawfal El Maguiri[3] · Hamza Essoussi[4] · Larbi Lasri[3] · Anthonin Demarbaix[5] · Rachid El Alaiji[1]

Received: 1 July 2025 / Accepted: 31 October 2025

Abstract

In this paper, physical and compression properties of 3D printed polyamide 12 (PA12) cylindrical parts are evaluated, and the impact of process parameters on these properties was analyzed. Within these parameters, a novel parameter is studied, powder heating temperature before printing, in order to examine its indirect effect on 3D parts. Firstly, compression samples were prepared by selective laser sintering (SLS) with controlled variations in laser power ratio, powder heating temperature and layer height. This preparation is carried out according to ASTM D695 standard of compressive test. Secondly, mass, volume, density and porosity were measured using a precision balance, Archimedes' principle and 3D scanning. Finally, compression tests are performed to determine compressive young's modulus, compression strength and fracture strain. The process variables that significantly affected the physical and mechanical properties were identified using analysis of variance (ANOVA). According to ANOVA results, physical and compression qualities are largely affected by the laser power ratio, rather than by layer height or powder heating temperature. High laser power, reduced layer height, and lower powder heating temperature significantly improved density while reducing porosity. Furthermore, the optimal configuration for improving mass, volume, compressive Young's modulus, and fracture strain is (3, 0.075 mm, 50 °C). However, the compressive strength, strain at break, and porosity of PA12 parts are all negatively affected by the following configuration: low laser power, high powder heating temperature, and medium layer height. Higher porosity, lower density, compression, Young's modulus, and strength are the result of material degradation. This degradation is attributed to overheating of the powder associated with an elevated laser power ratio and layer height. These findings highlight the importance of precise control of powder heating temperature, laser power, and layer height to optimize characteristics evaluated for polyamide performance.

Keywords Selective laser sintering · Polyamide 12 · Powder heating temperature · Laser power ratio · Layer height · Compression test · Porosity and density

✉ Fatima-Ezzahrae Jabri
fatimaezzahrae.jabri1@etu.uae.ac.ma

[1] Laboratory of Innovative Technologies (LTI), Abdelmalek Essaadi University, ENSA, Road Ziaten Km 10, Tangier Principale, BP: 1818, Tangier, Tangier 90060, Morocco

[2] Laboratory of Computer Science & Smart Systems (C3S), High school of technology, Hassan II University, EST, Road El Jadida Km 7, Casablanca, Casablanca 8012- Oasis, Morocco

[3] Systems Engineering and Innovation Laboratory, Mechanics and Systems Engineering Team, Moulay Ismail University, ENSAM, Marjane 2, B.P. 15290-Al Mansor, Meknes 50000, Morocco

[4] Arts & Métiers Innovation on Materials & Processes (AMI-MP) Research Team, AIDTM Laboratory, Moulay Ismail University, ENSAM, Marjane 2, B.P. 15290-Al Mansor, Meknes 50000, Morocco

[5] Science and Technology Research Unit, Haute Ecole Provinciale de Hainaut Condorcet, Boulevard Solvay 31, Charleroi 6000, Belgium

Published online: 17 November 2025

1 Introduction

Due to several production techniques, additive manufacturing has become more and more widespread across the industrial sector. Powder Bed Fusion (PBF), Material Extrusion (MEX), and VAT Photopolymerization (VPP) are a some of the 3D printing techniques available for this purpose [1]. Powder bed fusion techniques, such as selective laser sintering (SLS) of polyamide 12 (PA12), allow for the layer-by-layer creation of 3D-printed items from CAD models by fusing powdered materials with laser energy. Recent developments in this technology have brought SLS to the forefront of rapid prototyping, tooling processes, and manufacturing [2]. In this context, current research concentrates on improving material properties and processing parameters to produce high-quality parts. In relation to this, Zhang et al. [3] have looked at particle size distribution and discovered that reduced porosity and higher density are the results of smaller particles. As well as, the use of spherical particles enhances the dimensional accuracy of 3D printed parts, as found by Chatham et al. [4]. From another point of view, other work focused on powder reinforcement, guaranteeing good performance by adding fibers to the polyamide reinforcement. For that, Y. Liu et al. [5] claimed that reinforcing PA12 using carbon fibers results in maximum tensile strength as a result of strong matrix binding. Besides, Mousa et al. [6] pointed out that the modulus of elasticity and tensile strength of polyamide 12 parts are improved by the addition of glass beads; nevertheless, their ductility is reduced. However, Tan et al. [7] noted that the weight fraction of fibers affects both density and porosity. As the weight% of fiber-reinforced polymers rises, the densification rates, porosity, and pore sphericity are all negatively affected. On the other hand, different PA12 powders are known to have varying thermal behaviors and crystalline structures, so they require different processing parameters [8]. In this regard [9, 10], identified layer height, volumetric energy density (VED), scan spacing, area energy density (AED) and laser power as important factors impacting mechanical characteristics and porosity. Research in this area [11–13] has shown that increasing energy input results in denser component form, better elongation at break, and higher tensile strength. Hence, there is a positive correlation between energy density, part density, and mechanical characteristics. Conversely, particle combustion and process failure may result from an excessive laser energy density [14]. In contrast, mechanical properties can be significantly improved by appropriately reducing the layer height [15]. Based on [16], models can be constructed with a mass reduction of more than 20% while retaining surface texture qualities perfectly adapted to mechanical and qualitative requirements. Likewise, different materials are associated with varying energy requirements [17]. With the use of a powder pretreatment approach based on layer-wise infrared radiation, Chen et al. [18, 19] developed an optimal process for achieving a maximum tensile strength of approximately 85 MPa for polyetheretherketone (PEEK). Besides, Arai et al. [20] performed research into how the proportion of short glass fibers affected the tensile strength of SLS Polybutylene Terephthalate (PBT), finding that a fiber weight fraction of 30% provided the best mechanical performance. For polyamide 12, strength, modulus, and elongation are often enhanced by reducing scan spacing and speed [14]. Supporting these results [21, 22], indicated that weaker mechanical characteristics are caused by porosity. In this context, a high porosity level caused the samples to have a delicate failure mechanism, as defined by Morano et al. [23]. So, as stated by [24], small changes in powder temperature can greatly affect the mechanical properties of the part and therefore its porosity. According to Toth-Taşcău et al. [25], reduced porosity is a common result of rising energy densities. Likewise, elevated laser power has the potential to improve mechanical characteristics and decrease porosity, as demonstrated by El Magri et al. [26]. Otherwise, higher scanning speeds often result in greater porosity, as less energy is required, which affects particle coalescence during printing [27]. In this reference [28], as the layer height increases, stress relaxation also increases, but density and compressive strength both decrease. This means that process and powder parameter management is crucial for achieving low porosity and strong mechanical characteristics. Extensive research has shown that laser power, layer thickness and scanning speed are three main variables affecting porosity, density and mechanical qualities. However, no comprehensive analysis has been carried out on the effects of modifying powder heating temperature prior to printing. As a novel approach, the combined effects of layer height, powder heating temperature and laser power on the physical and compression characteristics of PA12 SLS cylindrical parts are investigated in this work. These physical characteristics comprise density, porosity, mass and volume. The aim is to determine whether these parameters can be used to reduce internal defects and enhance compression and physical characteristics of manufactured parts. The constraints and findings of combining powder heating temperature with laser power and layer height will be presented.

2 Methods and materials

2.1 Materials, SLS printer and sample preparation

An evaluation of SLS technique for nylon composites was conducted using Polyamide 12 smooth (PA12 smooth) powder. The powder, supplied by Seica (Élancourt, France), has an average particle size of 38 µm, in accordance with the specifications of ISO 13,220. In our study, cylindrical samples were

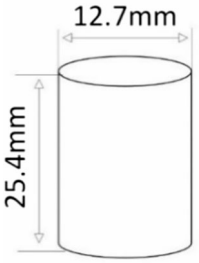

Fig. 1 PA12 specimen dimensional configuration

Table 1 Technical features of Sinterit Lisa printer [30]

3D printer	Sinterit Lisa printer
Size of print bed	150 × 200 × 150 mm
Powder type	PA12
Refresh ratio	22%
Laser type	IR Diode (5 W) on XY kinematics
Wavelength of laser	808 nm
Spot laser size	400 µm
Powder application system	Roller recoater with linear movement

manufactured following the ASTM D695 standard for compression testing. The cylinder measures 25.4 mm in height, and has a diameter of 12.7 mm, as illustrated at Fig. 1. All samples were therefore printed using an SLS 3D printer (Sinterit Lisa, Poland). Table 1 details the functional parameters of the Sinterit Lisa printer. Sinterit Lisa 2019 is utilized as the slicing software to produce G-code from STL files that are imported from CATIA V5.In addition, Fig. 2 shows the outcomes of the Differential Scanning Calorimetry (DSC) thermograms conducted by Olejarczyk et al. [29] on PA2200, PA12 Smooth, and PA12 Black powders. Since PA12 smooth is the material that our work is concerned with, it is the primary focus of this study. The results confirmed the structured nature of its crystals through DSC analysis. A single melting and crystallization peak was observed on the cooling and heating curves, with a melting temperature of 176.5 °C and a crystallization

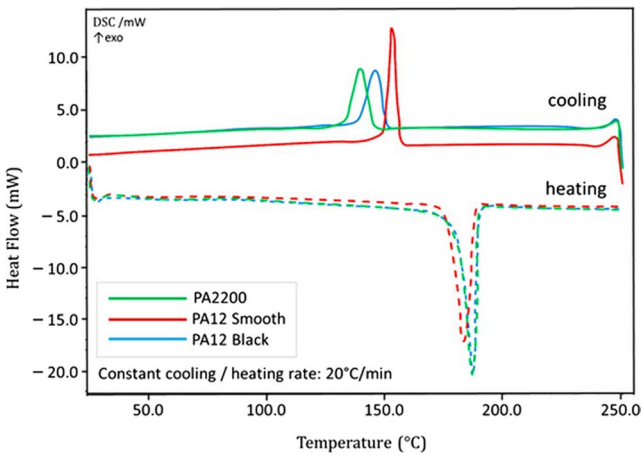

Fig. 2 Thermal behavior of PA2200, PA12 Smooth, and PA12 Black powders obtained by DSC (data from Olejarczyk et al.,2020 [29])

temperature of 157.4 °C. Since the greater melting enthalpy increases the thermal bleeding of unmelted particles, it allows for more exact contour melting [8].

2.2 Powder preparation

During SLS process, PA12 powder can be influenced by ambient humidity, which affects the chemical composition of the polyamide powder [31]. To address this issue, and in accordance with the technical specification sheet and supplier instructions, the powders must be stored in a sealed dry container. Furthermore, ten sachets of 1 g silicone absorber were integrated on the powder container to mitigate moisture absorption by the PA12 powder particles during the refresh step, thereby ensuring the powder's viability over prolonged periods. The powder was heated to three distinct temperatures for a duration of twenty-five minutes, as shown in Fig. 3. Figure 3 shows the subsequent 18-minutes process of sieving the powder using the Sinterit Powder Sieve. The powder is then prepared for printing after passing through the sieve. Dry powder is sieved and refreshed with 22% fresh powder each sample printing. The proportion of fresh powder was added in accordance with the instructions provided by the Sinterit Lisa printer to ensure optimal recycling. Amount of new powder to be added is shown on the printer's screen. The goal of this phase is to make the powder as uniform as possible by combining the used and fresh particles and reducing any fluctuations in particle size. This process is iterated for every single test scenario.

2.3 Process parameters and experimental procedure

The SLS settings cooperate three variations: powder heating temperature(25 °C,50 °C,75 °C), laser power ratio (1,2,3) and layer height(0.075 mm,0.125 mm,0.175 mm). Particularly, Sinterit Lisa printer enable a range of 0.5 to 3 for laser power ratio, which represents a multiplicative factor applied to the final laser power. In order to evaluate the impact of laser energy on the quality of printed parts, three levels were chosen to stay within the manufacturer recommended range. On the other hand, for the purpose of minimizing moisture absorption before printing, the Sinterit manufacturer recommends heating the powder to 50 °C. Because of this, we tested the effects of varying the powder heating temperature from 25 to 75 °C on the printed parts' characteristics, rather than keeping to the specified heating setting. All levels of each parameter were combined using a complete factorial approach, producing 27 different combinations. Low, medium, and high factor levels were determined for each parameter. Based on the data in Table 2, all other processing

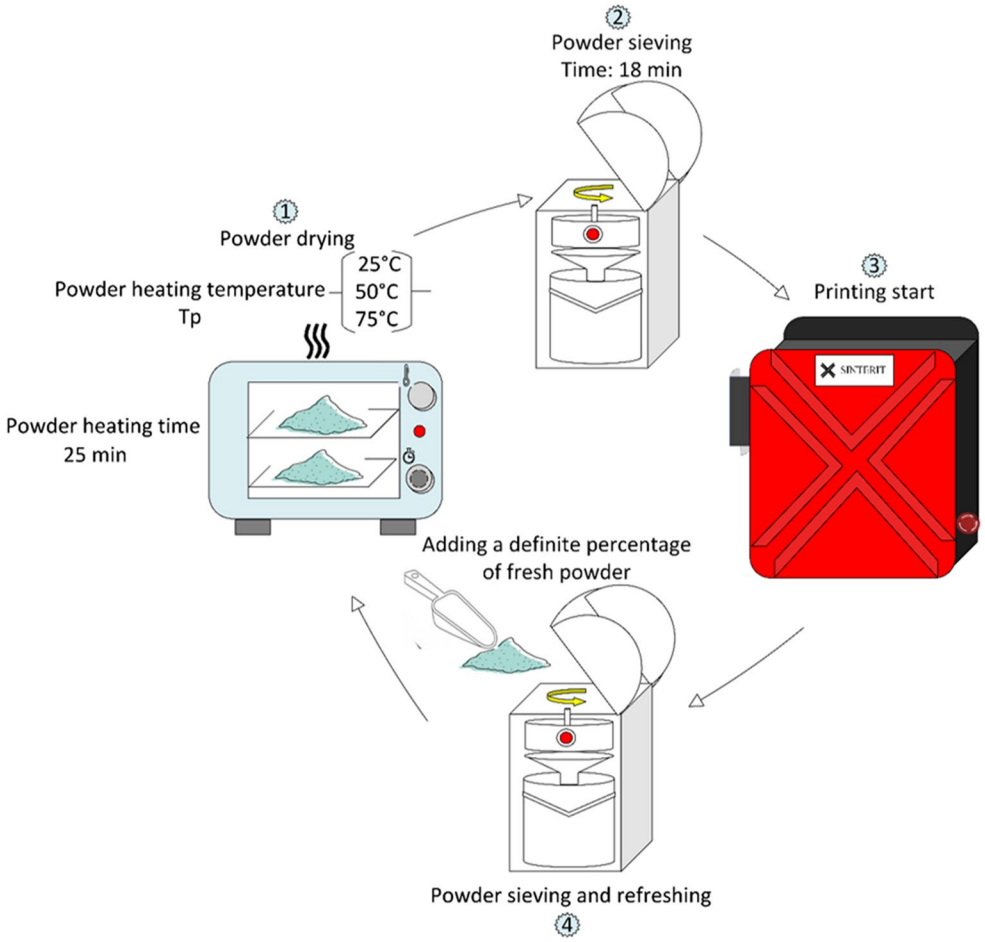

Fig. 3 Powder treatment processus

Table 2 Constant parameters of SLS PA-12 samples [30]

Non variable parameters	Values
Hatch spacing (mm)	0.36
Maximum laser power (W)	5
Build speed (mm/h)	3
Build chamber Temperature (°C)	178
Laser Spot Size (µm)	400
Preheating temperature (°C)	172
Print surface temperature (°C)	177.5
Printing direction	0/90°

parameters were kept constant. For each SLS test, three compression test specimens were consistently made under the identical circumstances to guarantee reliable findings. All variables and their respective build numbers are listed in Table 3.

2.4 Mass/volume/density/porosity

Prior to testing, several physical properties were quantified. The mass of the samples was measured after each printing experiment using a Sartorius balance (Fig. 4), model CP 323 P, which has a display accuracy of 0.001 g, external dimensions of 33 cm (D) x 15 cm (H) x 21.5 cm (W), and a tray diameter of 12 cm. The samples were scanned using UE11 3D Shining scanner (Fig. 5). It measures 298 mm x 90 mm x 74.5 mm. Accuracy to within 0.02 mm and a scanning speed of 1,350,000 points per second are its strong characteristics. The single-line scan mode was used to capture additional data for a more complete and accurate inspection. Scanners were aided by a data-capturing program that brought in raw Cartesian coordinate data. Hence, the ASCII format (. xyz or. Ptx) was employed to record the filtered point cloud data. Cloud scans were utilized to generate the model via 3D Systems' Geomagic Warp V2021 application. The total volume of the printed specimens was determined using Geomagic Control X V2020 software. Consequently, the density was calculated based on the relationship between mass and volume, as expressed in Eq. 1.

$$\rho = \frac{m}{V} \tag{1}$$

where *m* represents the mass of the part and V denotes the total volume of the part.

Porosity analysis was performed by applying the following equation of Archimedes principle [32] :

Table 3 Configuration of process parameter variations

Test case	Laser power ratio	Layer height (mm)	Powder heating temperature (°C)
1	1	0.075	25
2	1	0.075	50
3	1	0.075	75
4	1	0.125	25
5	1	0.125	50
6	1	0.125	75
7	1	0.175	25
8	1	0.175	50
9	1	0.175	75
10	2	0.075	25
11	2	0.075	50
12	2	0.075	75
13	2	0.125	25
14	2	0.125	50
15	2	0.125	75
16	2	0.175	25
17	2	0.175	50
18	2	0.175	75
19	3	0.075	25
20	3	0.075	50
21	3	0.075	75
22	3	0.125	25
23	3	0.125	50
24	3	0.125	75
25	3	0.175	25
26	3	0.175	50
27	3	0.175	75

Fig. 4 Measurement of Sample Mass

$$\epsilon = 100 * \left(1 - \frac{\rho}{\rho_{theoretical}}\right) \quad (2)$$

In this equation, ε signifies total porosity, $\rho_{theoretical}$ is the theoretical density of the fully dense material, which is 1.02 g/cm³ [33, 34], and ρ is the measured density of the part.

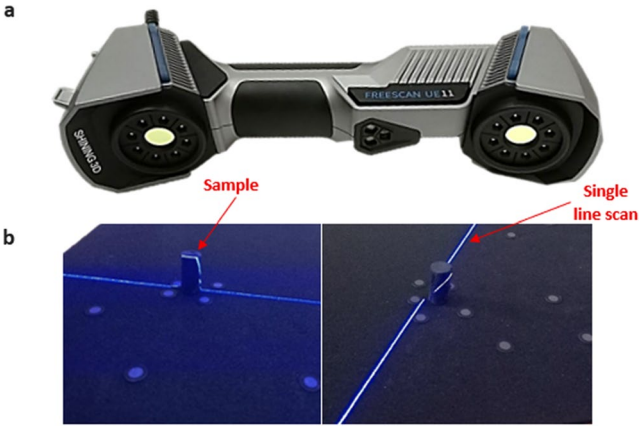

Fig. 5 (**a**) 3D Shining scanner UE11 (**b**) 3D Scanning of a Cylindrical Sample

2.5 Compression test

To examine the mechanical properties of the samples, including compressive young's modulus (Ec in GPa), compressive strength (σ_M in MPa), and fracture strain (ϵ_M in %), compression tests were conducted in accordance with ASTM D695 standards. Ec represents the relationship between stress and strain in the elastic region. In addition, σ_M refers to maximum stress that material can withstand before breaking. ϵ_M denotes deformation of sample when it reaches its maximum compressive strength. Besides, the tests were performed at a rate of 1.3 mm/min using a Zwick/Roell Z050 testing machine, which has a maximum load capacity of 50 kN. A 40% crushing load was steadily increased till failure for each specimen. Testing data was taken in real time using TestXpert. Figure 6 depicts the testing machine. An analysis of variance (ANOVA) was used to examine the statistical significance of process parameters (powder heating temperature, laser power ratio, and layer height) on measured responses. Using the ANOVA results, the parameters that had the biggest impact on mechanical and physical attributes were determined.

3 Results and discussions

In this research, 3D cylindrical PA12 parts were examined for the physical and compressive characteristics. The first properties studied with this cylindrical part were porosity, density, volume, and mass. Then followed by the compression properties, which involved values of Young's modulus, compressive strength, and fracture strain. The primary goal was to ascertain the effect of powder heating temperature on these SLS PA12 part features as it relates to laser power and layer thickness. In this section, the particulars of these

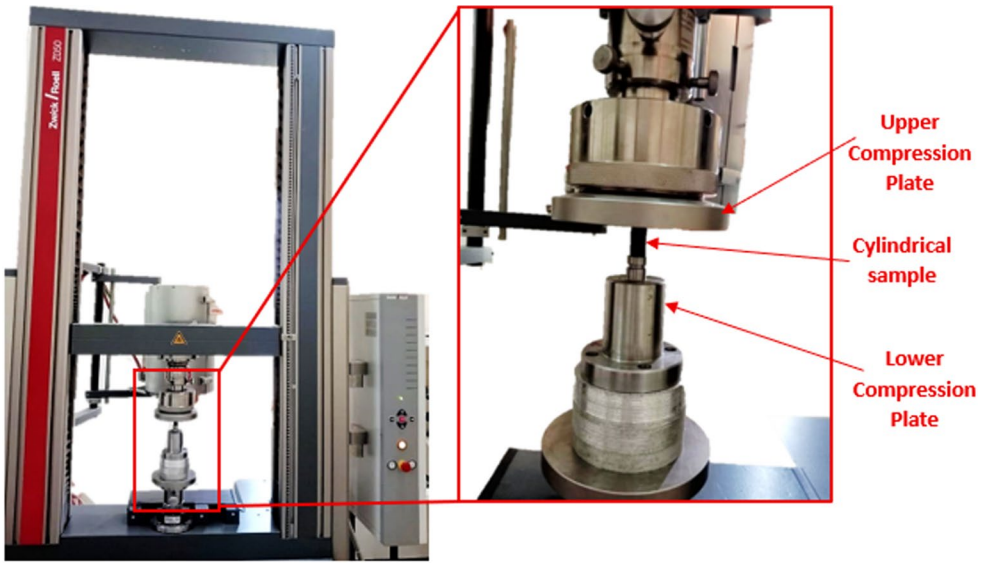

Fig. 6 Compression Test Setup for PA12 SLS parts

experiments, the associated findings, and the indirect effects of powder heating temperature are discussed.

3.1 Mass/volume/density/porosity

Table 4 shows the average mass, volume, density and porosity of 3D printed parts under different combinations of laser power ratio, layer height and powder heating temperature (with standard deviation indicated between brackets). The optimal print settings for density and porosity include a laser power ratio of 3, a layer height of 0.075 mm, and a powder heating temperature of 25 °C (Combination 19). This is due to the synergistic effect of low powder heating temperature and increased laser power. So, this shows that increasing the laser power ratio while reducing the layer height and powder heating temperature results in higher density and lower porosity. In this regard, this brings density closer to the predicted PA12 density of 1.020 g/cm³, with an inaccuracy of 0.0010 g/cm². Furthermore, minimal powder heating temperature results in preventing excessive thermal input, and tiny layer height improves the consistency of layer bonding. According to Azam et al. [17], creating denser components is made easier by enhancing laser power. Besides, decreased mass is attained with low laser power, increased layer height and powder heating temperature for run no 9. This suggests that increased powder heating temperature didn't compensates for low laser power for increased layer height resulting in minimal particle melting and reduced mass. Based on the volume data, the sample number 2 of a low laser power ratio and layer height and a medium powder heating temperature (1, 0.075 mm, 50 °C) generates a volume value that comes closest to the CAD reference volume of 3.22 cm³ is 3.18 cm³. These settings allow regulated polymer sintering due to moderate heating temperature input and fine layer height. On the other hand, the volume can be significantly lowered by decreasing the values of layer height, powder heating temperature, and laser power, when using configuration 1 (1, 0.075 mm, 25 °C). The minimum volume results from inadequate thermal activation of the polymer powder at minimal values of powder heating temperatures and laser power, preventing effective sintering. The decreased layer height exacerbates the effects of thermal instabilities, leading to considerable shrinkage and a marked decrease in the final volume of the part.

3.1.1 Indirect impact of powder heating temperature

Figure 7 illustrates how powder heating temperature affects the mass, volume, density and porosity of 3D printed parts. Samples with a layer height of 0.075 mm and a powder heating temperature of 50 °C achieve maximum mass, as seen in Fig. 7(a). This implies that moderate powder heating temperatures, such as 50 °C, correctly balance heat input and deposition stability. In this context, porosity reduces and density increases at 50 °C for 1 or 2 of laser power with 0.125 mm of layer height, as shown in Fig. 7(h, k). From 25 °C to 75 °C of powder heating temperature, specimen mass decreases steadily with a laser power ratio of 1 and a layer height of 0.125 mm (see Fig. 7(b)). In this regard, higher powder heating temperatures under lower laser power and medium layer height reduce part mass. High laser power ratio configurations (0.075 mm, 3 and 0.175 mm, 3) in Fig. 7(g, j, i, l) exhibit an increased trend in porosity and a decrease trend in density as powder heating temperature increases. For that, increasing the powder heating temperature and laser power can cause the material to lose its structural cohesiveness due to overheating. It is stated in [35] that excessively high melting temperatures significantly accelerate material failure. In

Table 4 Physical properties results: mass, volume, density and porosity

Test case	Average part mass (g)	Volume average (cm3)	Density calculated average (g/cm3)	Total Porosity average (%)
1	2.864 (+/−0.075)	**2.97 (+/−0.08)**	0.964 (+/−0.001)	5.515 (+/−0.063)
2	2.950 (+/−0.063)	3.18 (+/−0.01)	0.928 (+/−0.020)	8.984 (+/−1.947)
3	2.925 (+/−0.065)	3.13 (+/−0.05)	0.935 (+/−0.010)	8.331 (+/−0.971)
4	2.882 (+/−0.076)	3.14 (+/−0.07)	0.917 (+/−0.016)	10.050 (+/−1.607)
5	2.790 (+/−0.076)	2.97 (+/−0.05)	0.938 (+/−0.012)	8.018 (+/−1.211)
6	2.786 (+/−0.077)	3.14 (+/−0.12)	**0.889 (+/−0.024)**	**12.875 (+/−2.348)**
7	2.771 (+/−0.054)	3.11 (+/−0.05)	0.891 (+/−0.022)	12.612 (+/−2.146)
8	2.778 (+/−0.046)	3.11 (+/−0.07)	0.893 (+/−0.002)	8.288 (+/−0.193)
9	**2.766 (+/−0.049)**	3.05 (+/−0.03)	0.906 (+/−0.014)	11.195 (+/−1.361)
10	3.533 (+/−0.074)	3.53 (+/−0.05)	1.001 (+/−0.011)	1.896 (+/−1.098)
11	3.574 (+/−0.104)	3.54 (+/−0.08)	1.011 (+/−0.007)	0.914 (+/−0.669)
12	3.461 (+/−0.053)	3.40 (+/−0.05)	1.018 (+/−0.002)	0.207 (+/−0.185)
13	3.454 (+/−0.081)	3.64 (+/−0.11)	0.949 (+/−0.007)	6.994 (+/−0.679)
14	3.604 (+/−0.065)	3.59 (+/−0.07)	1.005 (+/−0.001)	1.494 (+/−0.119)
15	3.495 (+/−0.091)	3.70 (+/−0.03)	0.944 (+/−0.020)	7.455 (+/−1.969)
16	3.444 (+/−0.046)	3.45 (+/−0.04)	0.999 (+/−0.000)	2.062 (+/−0.046)
17	3.410 (+/−0.070)	3.43 (+/−0.08)	0.995 (+/−0.004)	2.451 (+/−0.373)
18	3.421 (+/−0.091)	3.42 (+/−0.10)	0.999 (+/−0.002)	2.038 (+/−0.203)
19	3.643 (+/−0.015)	3.58 (+/−0.01)	**1.019 (+/−0.001)**	**0.095 (+/−0.069)**
20	3.658 (+/−0.071)	3.62 (+/−0.06)	1.011 (+/−0.009)	0.905 (+/−0.867)
21	3.600 (+/−0.041)	3.62 (+/−0.12)	0.996 (+/−0.025)	2.339 (+/−2.424)
22	3.854 (+/−0.073)	3.91 (+/−0.09)	0.985 (+/−0.009)	3.458 (+/−0.856)
23	3.872 (+/−0.099)	3.86 (+/−0.06)	1.003 (+/−0.010)	1.687 (+/−1.005)
24	3.810 (+/−0.097)	3.81 (+/−0.13)	1.000 (+/−0.011)	1.923 (+/−1.051)
25	3.962 (+/−0.103)	3.90 (+/−0.11)	1.017 (+/−0.003)	0.273 (+/−0.296)
26	**4.030 (+/−0.149)**	**3.98 (+/−0.16)**	1.014 (+/−0.003)	0.602 (+/−0.278)
27	3.894 (+/−0.107)	3.91 (+/−0.13)	0.996 (+/−0.010)	2.338 (+/−0.998)

contrast, for combinations such as (0.075 mm, 2) depicted in Fig. 7 (g, i), higher powder temperatures reduce porosity and increase density. Higher powder heating temperatures for this combination improve material flow and interlayer adhesion, particularly at reduced layer heights and medium laser power ratio, which explains the observed decrease in porosity and increase in density. These results underscore the crucial function of powder heating temperature in controlling material behavior during the printing process. It regulates the flow and fusion temperatures, which, combined with parameters including layer height and laser power ratio, that influence directly the physical characteristics of 3D printed parts.

Physical variables such as volume, density, porosity and mass were subjected to an analysis of variance (ANOVA) to determine the most important factor affecting processing. According to the results presented in Table 5, the laser power ratio had the greatest effect on the mass, volume, density and porosity of 3D printed parts (high F-value and low P-value). It seems that the physical properties of printed part are unaffected by heating temperature since it is linked to the lowest F values. Nevertheless, the volume, density, and porosity are greatly impacted by the interaction of layer height with powder heating temperature, since this interaction exhibits higher values of F compared to other interaction. On the flip side, the mass of PA 12 parts is heavily influenced by the interplay of all parameters, such as the laser power ratio, layer height, and powder heating temperature.

3.2 Mechanical properties

The mechanical properties demonstrate significant variances in performance across test configurations (Table 6). The compressive young's modulus reached its maximum at (2/0.075 mm/25°C) and measured 0.186 GPa. Nonetheless, a value of 0.085 GPa was reported as the lowest, at (1/0.175 mm/25°C). Additional energy delivered with a medium laser power ratio combined with thinner layer height result in increased stiffness, which enhances particle sintering [15, 36]. Since 25 °C is enough to prevent overheating, particularly with minimal layer height, medium laser power compensates for the powder heating temperature role in this case. The compressive young's modulus is lowered as energy is decreased particularly with greater layer height. Another factor contributing to this reduction is the combination's porosity value (12.612%), which results in low

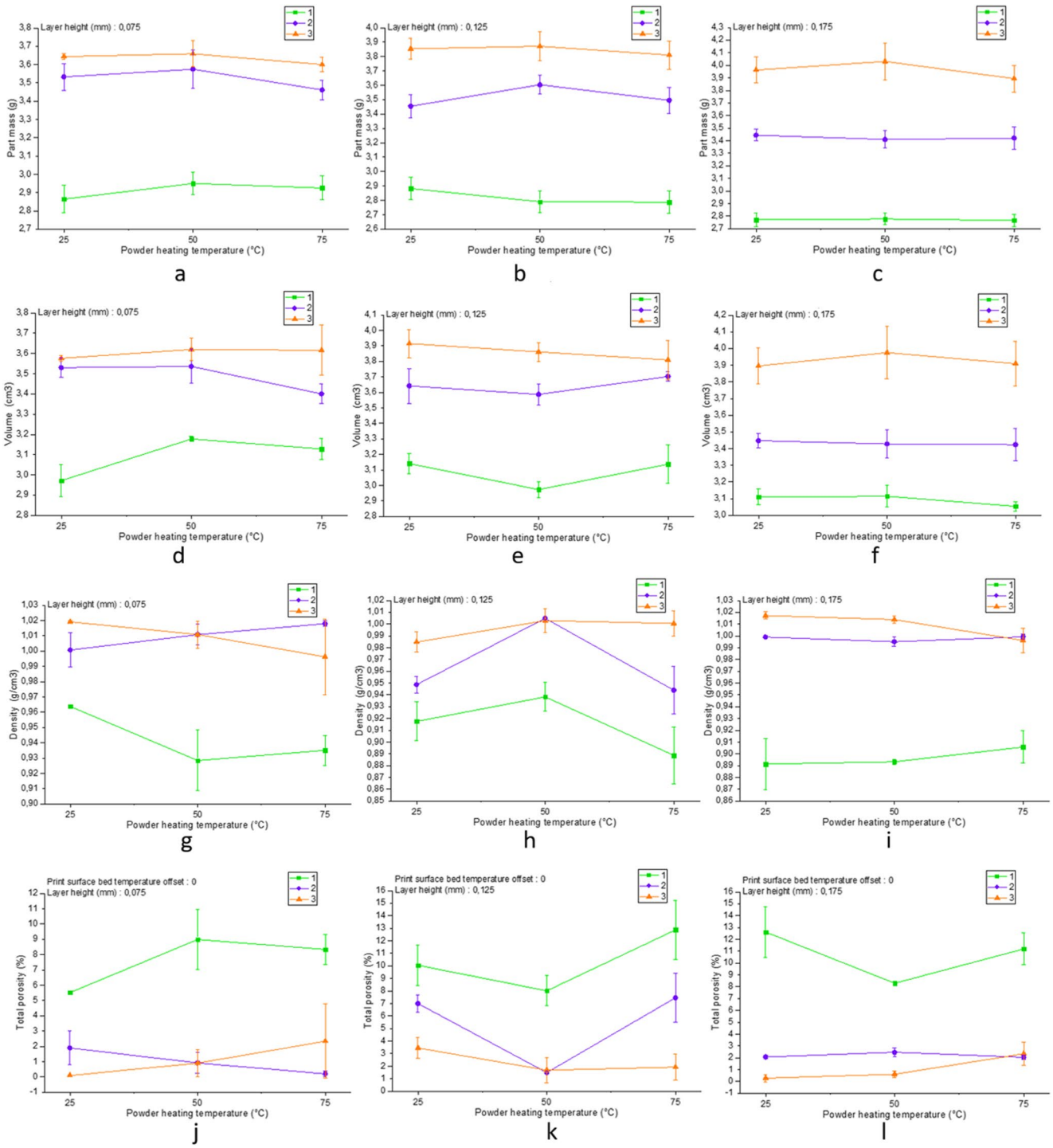

Fig. 7 **(a, b, c)**: Mass as function of powder heating temperature. **(d, e, f)**: Volume as function of powder heating temperature. **(g, h, i)**: Density as function of powder heating temperature. **(j, k, l)**: Porosity as function of powder heating temperature

compressive young's modulus. Porosity is the cause of the poorest mechanical characteristics, as mentioned in [21]. Furthermore, the highest compressive strength of 68.151 MPa was achieved using less powder heating temperatures (3/0.175 mm/25°C), greater laser powers, and thicker layer heights. The increased strength is due to the lower porosity (0.273%), which is caused by the increased laser power (3). Another study reinforced these findings by reporting that raising laser power minimized porosity [14]. The lowest compressive strength, however, is found at 1/0.125 mm/75°C, due to the high percentage of porosity, which is the actual cause of the

Table 5 ANOVA results for physical properties of SLS PA12 parts

Source	Mass		Volume		Density		Porosity	
	F- value	*P*- value	F- value	*P*- value	F- value	*P*- value	F- value	*P*-value
Laser power ratio	43.01	0.002	28.19	0.004	26.98	0.005	42.03	0.002
Layer height	0.07	0.935	1.04	0.433	2.55	0.193	4.3	0.101
Powder heating temperature	0.14	0.875	0.01	0.994	0.5	0.639	1.69	0.294
Laser power ratio*Powder heating temperature	0.02	0.998	0.03	0.997	0.19	0.933	0.27	0.885
Layer height*Powder heating temperature	0	1	0.18	0.94	0.69	0.638	1.01	0.495
Laser power ratio*Layer height*Powder heating temperature	0.05	1	0.12	0.994	0.34	0.908	0.79	0.64

Table 6 Results of mechanical properties of each combination

Test case	Mean Compressive young's modulus Ec (GPa)	Mean Compressive strength σM (MPa)	Mean Fracture strain εm (%)
1	0.086 (+/−0.017)	47.342 (+/−6.291)	19.605 (+/−2.422)
2	0.120 (+/−0.044)	55.427 (+/−3.829)	21.175 (+/−2.188)
3	0.141 (+/−0.013)	49.296 (+/−13.694)	21.325 (+/−3.313)
4	0.131 (+/−0.048)	40.321 (+/−1.163)	18.337 (+/−0.284)
5	0.087 (+/−0.025)	33.238 (+/−4.984)	15.495 (+/−2.035)
6	0.090 (+/−0.017)	**19.664 (+/−2.829)**	13.418 (+/−1.346)
7	**0.085 (+/−0.038)**	29.375 (+/−9.188)	14.702 (+/−3.594)
8	0.103 (+/−0.012)	28.223 (+/−2.336)	13.921 (+/−1.631)
9	0.108 (+/−0.069)	24.881 (+/−1.158)	12.426 (+/−0.410)
10	**0.186 (+/−0.008)**	60.683 (+/−3.701)	19.695 (+/−2.202)
11	0.168 (+/−0.023)	66.054 (+/−6.447)	22.663 (+/−3.456)
12	0.184 (+/−0.016)	65.566 (+/−4.175)	21.483 (+/−2.558)
13	0.118 (+/−0.098)	52.814 (+/−2.285)	17.264 (+/−3.693)
14	0.151 (+/−0.020)	57.974 (+/−0.087)	23.202 (+/−0.379)
15	0.148 (+/−0.003)	39.528 (+/−4.793)	**11.987 (+/−5.203)**
16	0.109 (+/−0.003)	50.967 (+/−5.172)	19.933 (+/−5.248)
17	0.160 (+/−0.016)	56.233 (+/−2.141)	24.211 (+/−0.342)
18	0.146 (+/−0.023)	52.376 (+/−3.196)	**27.146 (+/−8.270)**
19	0.163 (+/−0.026)	61.763 (+/−2.213)	20.554 (+/−1.796)
20	0.163 (+/−0.002)	55.095 (+/−2.058)	15.849 (+/−2.623)
21	0.161 (+/−0.010)	49.777 (+/−0.454)	13.884 (+/−1.064)
22	0.160 (+/−0.004)	53.097 (+/−2.575)	18.956 (+/−0.878)
23	0.141 (+/−0.027)	55.061 (+/−2.046)	18.028 (+/−1.162)
24	0.147 (+/−0.012)	54.798 (+/−2.957)	20.007 (+/−2.904)
25	0.141 (+/−0.028)	**68.151 (+/−5.451)**	26.621 (+/−6.832)
26	0.148 (+/−0.030)	67.898 (+/−7.654)	27.077 (+/−7.854)
27	0.108 (+/−0.005)	64.072 (+/−2.561)	26.852 (+/−2.641)

strength loss [21]. On the other hand, the fracture strain values varied between 27.145% at (2/0.175 mm/75°C) to 11.987% at (2/0.125 mm/75°C). Superior ductility is achieved by maintaining the layer height at 0.125 and 0.175 mm, which balances the high powder heating temperature against the medium laser power ratio.

3.2.1 Impact of powder heating temperature on compression young's modulus

Figure 8 displays the analysis of the compression young's modulus as a function of powder heating temperature. Depending on combinations, trends respond differently to changes in powder heating temperature, indicating different parameter interaction effects. For example, many combinations (e.g., 0.075 mm/2, 0.125 mm/1, 0.125 mm/3) display a downward trend initially, followed by a rise (refer to Fig. 8(b, d, f)). This pattern indicates that in 25 °C of powder heating temperature, compression young's modulus improvements are more pronounced for setups with lower and medium layer thickness. This response aligns with findings in [37] claimed that lower layer thickness improves the mechanical properties. In contrast, combinations with a high layer thickness (e.g., 0.175 mm) often show an increase in compression young's modulus, followed by a decrease as powder heating temperature rises, as seen in setups like 0.175 mm layer height and 3 laser power ratios, illustrated in Fig. 8(i). This indicates that high laser power improves compressive young's modulus at medium powder heating temperatures especially 50 °C due to sufficient energy absorption and bonding. At 50 °C, maximum mass and volume are obtained which further explain the increase of compression young's modulus of this combination. An paper published by [36] provided evidence that the use of elevated laser power enhances particle sintering and young's modulus. However, thermal degradation or overheating can reduce compression properties as powder heating increases, particularly with rising laser power and layer height (0.175 mm/3). However, combination with a thin layer height and a high laser power ratio (e.g., 0.075 mm/3 as captured in Fig. 8 (c)) show a consistent trend, suggesting that further increases in powder heating temperature have little effect at these settings. This is probably due to the fact that higher laser power optimizes bonding efficiency. Conversely, combinations in Fig. 8 (a, g) with low laser power ratios (e.g. 0.075 mm/1, 0.175 mm/1) show a tendency to increase. This could be due to the increase in powder heating temperature, which results in higher energy input rather than laser power. These results underline the crucial role of the interaction between layer thickness and laser power in regulating interlayer bonding. In addition, some combinations show optimal compression young's modulus in different powder heating temperature ranges.

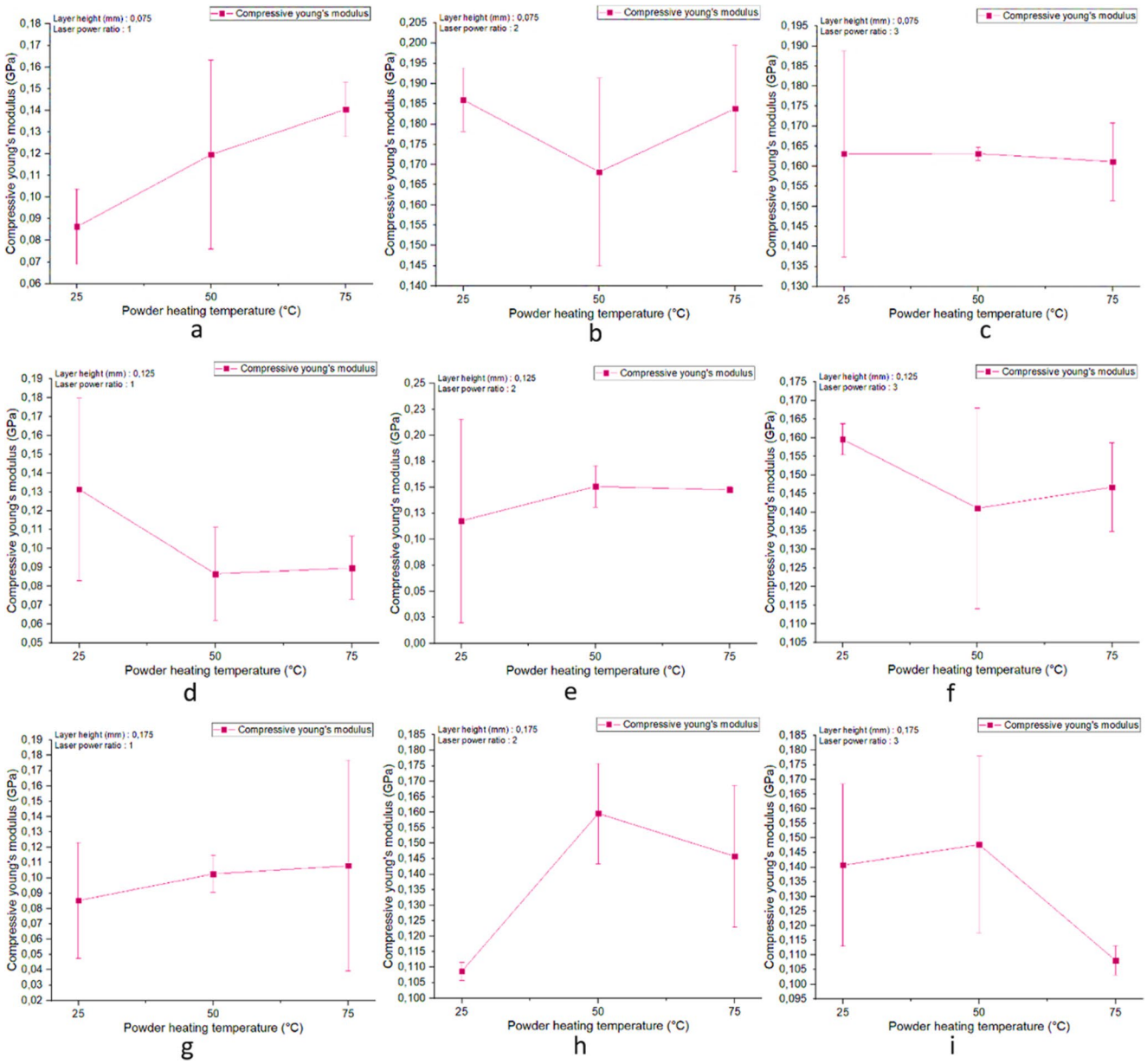

Fig. 8 **(a, i)**: Variation of Compressive young's modulus with powder heating temperature

Table 7 displays the results of the F-value and p-value analysis conducted on the compression young's modulus of 3D printed parts. According to the F-value, the two most important criteria for compression young's modulus are laser power and layer height. The results also show that the most significant variables in the model with P values less than 0.05 are laser power and layer thickness. On the other hand, powder heating temperature is thought to have a minimal effect. Besides, the F-value shows that compressive young's modulus interacts most strongly with powder heating temperature, layer height, and laser power configuration.

Table 7 ANOVA results for compressive young's modulus of SLS PA12 parts

Source	Compressive young's modulus	
	F- value	*P*-value
Laser power ratio	24.92	0.006
Layer height	8.9	0.034
Powder heating temperature	0.51	0.637
Laser power ratio*Powder heating temperature	1.43	0.37
Layer height*Powder heating temperature	1.4	0.376
Laser power ratio*Layer height*Powder heating temperature	1.78	0.302

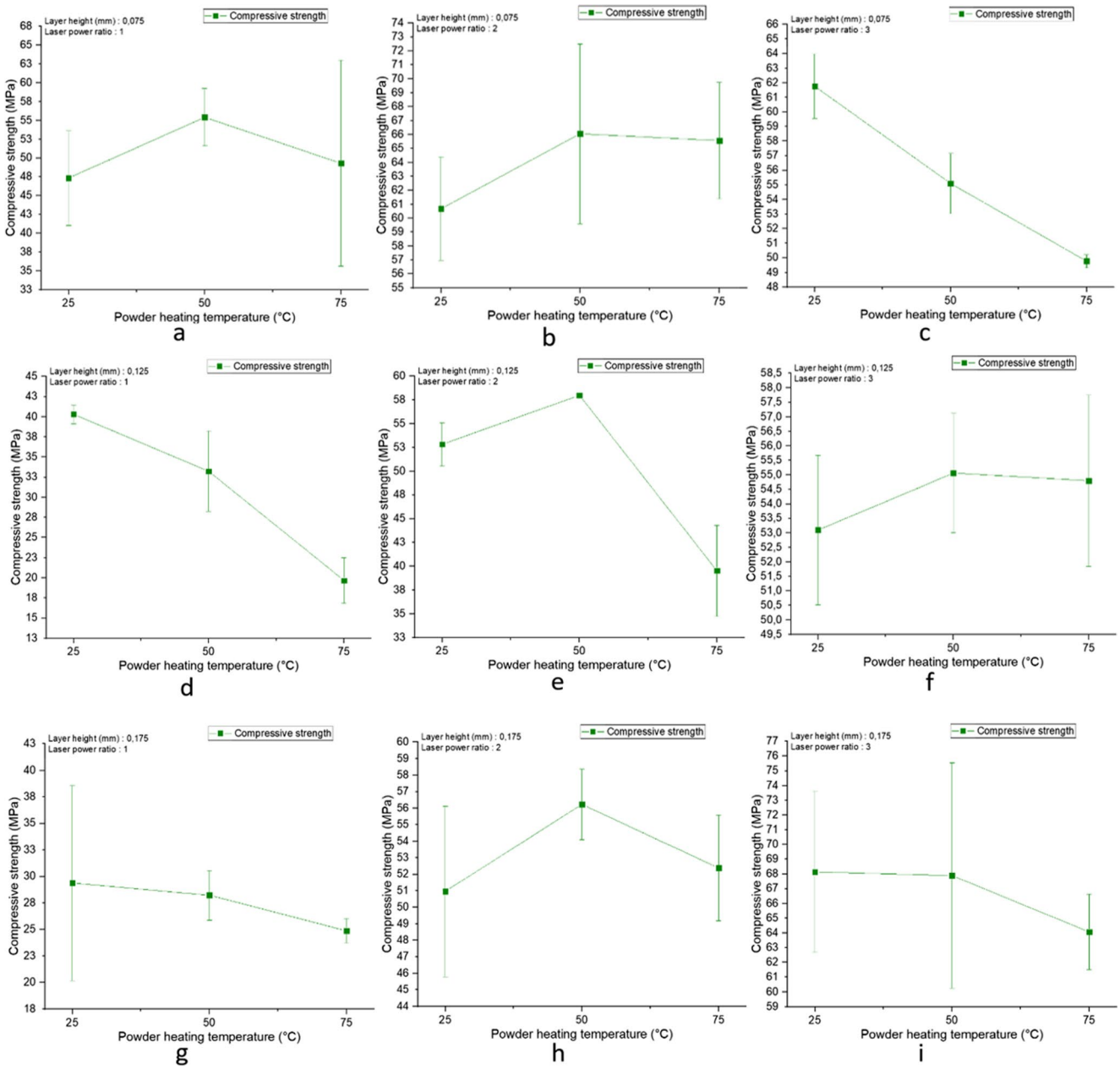

Fig. 9 (a, i): Effect of Compressive strength on powder heating temperature levels

3.2.2 Impact of powder heating temperature on compressive strength

The analysis of compressive strength in relation to powder heating temperature reveals a complex interplay among layer height and laser power ratio (Fig. 9). Most figures indicate a rising trend in compressive strength followed by a decrease as the powder heating temperature increase. For instance, at these configurations in Fig. 9(a, b, e, f, h) like (0.075 mm, 1), (0.075 mm, 2), (0.125 mm, 2), (0.125 mm, 3) and (0.175 mm, 2), compressive strength improves significantly at 50 °C. This pattern suggests that 50 °C powder heating temperature for these combinations plays the role of laser power. As with reduced values of layer height and laser power, 50 °C of powder heating temperature compensates for the minimum laser power. Also, due to the optimal volume obtained for this combination 3.18 cm^3 that contributes on improved compressive strength. In this respect, low values of laser energy prevent particle mixing and minimize the mechanical strength of the printed parts as noted by [38]. However, for medium and high levels of layer height, and laser power, laser power is not enough for good sintering. Therefore, for this configuration, 50 °C of powder heating temperature support laser power in improving the

compressive strength of the 3D printed parts. In addition, Fig. 9 (d, g, i, c) presents a downward trend observed at medium and maximum layer height settings (e.g., 0.125 mm/1, 0.175 mm/1,0.175 mm/3) and at reduced layer height combined with elevated laser power (e.g., 0.075 mm/3). This reveal that elevated powder heating temperature for reduced laser power and medium or elevated layer height impacts negatively compressive strength due to thicker layer height that broken the positive effect of powder heating temperature. Also, reduced mass, volume and density and increased porosity obtained at Table 4 are the reason behind this decline. In terms of this, laser power and layer height were shown to have the greatest impact on mechanical characteristics [39]. As well as, improved levels of laser power and layer height reduce compressive strength as powder heating temperature rises. Likely due to excessive heat buildup that may compromise the material's structural integrity. The same impact is observed for high laser power and reduced layer thickness because of excessive energy created by high levels of laser power and powder heating temperature. Thus, understanding these parameter interactions is crucial for optimizing compressive strength in SLS 3D printing.

The results of the analysis of variance (ANOVA) are summarized in Table 8. Compressive strength was found to be low impacted by powder heating temperature or layer height, according to the computed p and F values. Nevertheless, there is strong evidence that the interplay between these three parameters significantly affects compressive strength, as seen by the higher F- value than other interactions. Conversely, laser power ratio has a clear impact on compressive strength as shown with higher F-value.

3.2.3 Impact of powder heating temperature on fracture strain

Figure 10 shows that powder heating temperature affects fracture strain differently depending on powder heating temperature, layer height and laser power ratio. Both the nominal and corrected values of the fracture strain are presented in Fig. 10. This gives a better picture of the difference between the original strain measurement and the adjusted data, which takes experimental adjustments into consideration. Both the corrective and nominal fracture strain curves yielded similar results. There is a noticeable decline in figures with high layer height as the temperature of powder heating rises. For example, configurations like (0.175 mm/1, 0.125 mm/1), illustrate this decline (see Fig. 10(g, d)). This trend suggests that greater layer thickness and low laser power impedes flexibility due to inadequate layer bonding, leading to decreased fracture strain at higher powder heating temperatures. Wu et al. [15]supports that the mechanical properties can be improved significantly when we reduced the layer thickness appropriately. As well as, the combination of reduced layer thickness and higher laser power results in a downward trend as powder heating rises. This is attributed to a rise trend obtained at porosity which explain that this combination rises the porosity percentage and drops fracture strain due to excessive energy produced from laser power and powder heating temperature. Conversely, an upward trend appears at lower laser power ratio. Configurations depicted in Fig. 10 (a) like 0.075 mm layer height and 1 laser power ratio, show this rise. This indicates that medium or higher powder temperatures with low energy input and thinner layer enable efficient sintering while preserving material flexibility [17]. confirms that preheating the powder chamber helps in minimizing the laser power required to melt the powder. Additionally, several combinations display an initial increase in fracture strain, followed by a decrease with rising powder heating temperature. This pattern is prominent at high and medium laser power ratio (refer to Fig. 10(i, b, e)), as seen in configurations like (0.175 mm/3, 0.075 mm/2, 0.125 mm/2). These trends suggest that while medium or high laser power ratio enhance strain initially due to strong interlayer bonds particularly at 50 °C of powder heating temperature. However, excessive powder heating temperature and laser power reduces strain by making the material brittle. At low powder heating temperatures and layer heights, the thinner layer may become more flexible, leading to an initial improvement in deformation. Nonetheless, the material can become too stiff and less flexible if the powder heating temperature is increased further. On the other hand, distortion at break decreases and then increases with increased laser power and medium layer height. It appears that inadequate bonding limits deformation at medium layer height. Nevertheless, deformation is positively influenced at higher levels due to improved adhesion between layers as the powder heating temperature increases.

Table 8 ANOVA results for compressive strength of SLS PA12 parts

Source	Compressive strength	
	F- value	*P*-value
Laser power ratio	5.84	0.065
Layer height	1.37	0.351
Powder heating temperature	0.42	0.684
Laser power ratio*Powder heating temperature	0.06	0.991
Layer height*Powder heating temperature	0.09	0.979
Laser power ratio*Layer height*Powder heating temperature	0.13	0.993

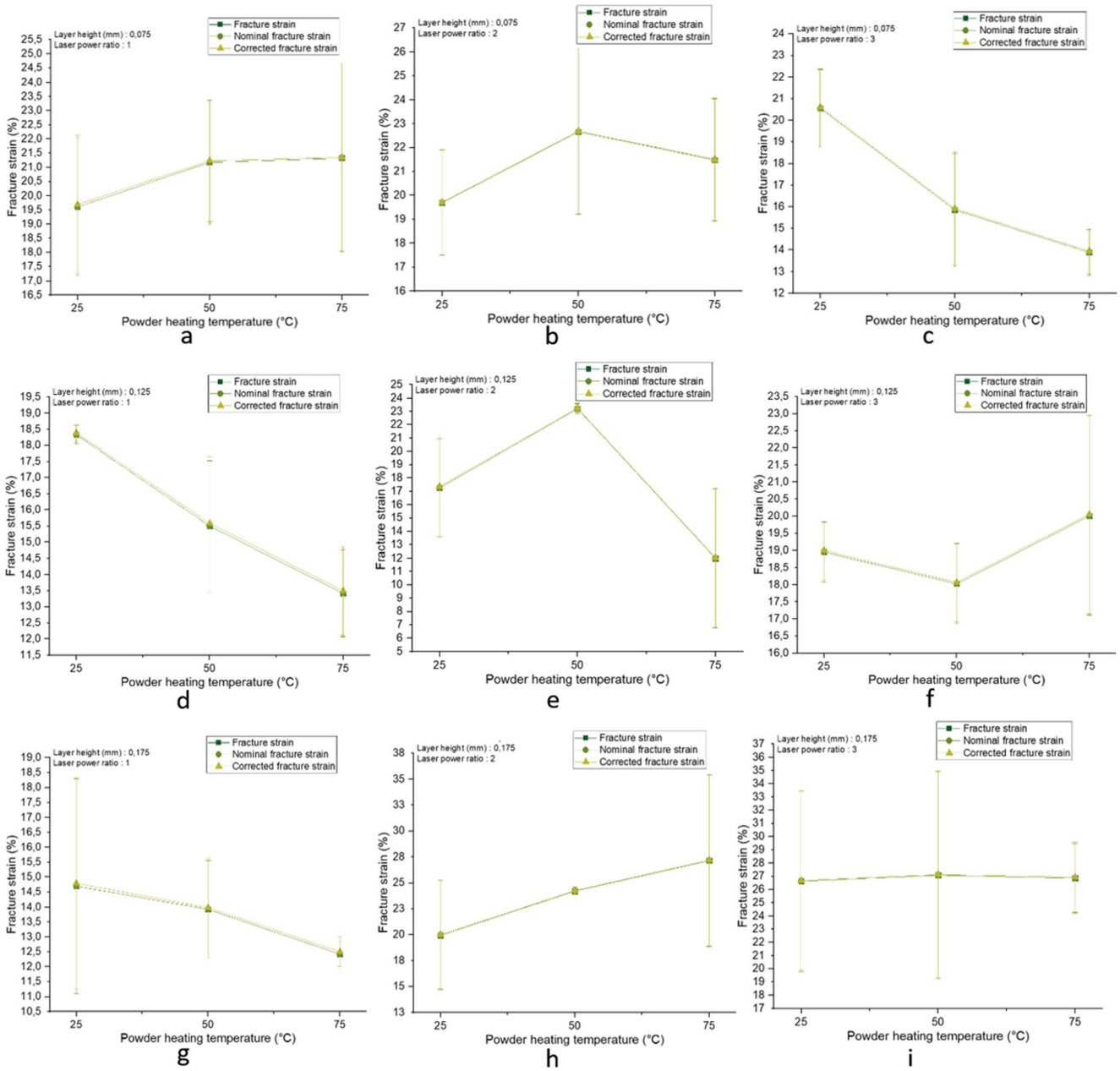

Fig. 10 **(a, i)**: Variation of fracture strain with powder heating temperature

Table 9 ANOVA results for fracture strain of SLS PA12 parts

Source	Fracture strain	
	F- value	*P*-value
Laser power ratio	0.88	0.481
Layer height	0.62	0.581
Powder heating temperature	0.08	0.923
Laser power ratio*Powder heating temperature	0.14	0.959
Layer height*Powder heating temperature	0.09	0.98
Laser power ratio*Layer height*Powder heating temperature	0.16	0.987

To further examine the fracture deformation data, analysis of variance (ANOVA) was employed (see Table 9). According to the F-value, the two parameters that contribute the most significantly to fracture deformation are laser power and layer height. However, the temperature at which the powder is heated has insignificant impact on fracture deformation. It is also clear from the decreased F-value that the interaction between layer height and powder heating temperature does not significantly affect fracture strain.

4 Conclusion

This paper investigated physical and compression responses of selective laser sintered PA12 polyamide, considering different levels of powder heating temperature, laser power and layer height. Physical and compression properties include mass, volume, density, porosity, compressive young's modulus, compression strength, fracture strain at compression test. For this purpose, three levels of each parameter were considered for cylindrical samples preparation. Results indicate that physical and compression properties are influenced by print parameters. Based on ANOVA finding, the most influential factor in physical and compression properties is the laser power ratio, followed by the layer height. The least critical factor is the temperature at which the powder is heated. However, there are combinations that have a greater impact on these properties. Hence, a layer height of 0.075 mm, an increased laser power, and a medium powder heating temperature are the optimal parameters for reaching maximum values in terms of volume, compressive Young's modulus, fracture strain, and mass. This suggests that moderate thermal conditions enhance deposition stability, with 50 °C and 0.075 mm being the ideal powder heating temperature and layer height for maximum mass, respectively. Conversely, components characteristics is negatively affected by lower laser power and higher powder heating temperature and medium layer height, leading to lower compression strength, greater porosity, and fracture strain. A dense part with reduced porosity was achieved with this parameter selection: (3, 0.075 mm, 25 °C). Increasing the laser power ratio, layer height, and powder heating temperature may potentially weaken the material and accelerate its degradation. Selection of print settings is necessary to achieve the desired physical and compression properties of 3D printed products. Future research should introduce other levels of powder heating temperature to better understand its role in porosity formation and mechanical response. To analyze how this parameter directly affects porosity creation and distribution in the part and their effect on mechanical properties.

Funding Not applicable.

Declarations

Ethics approval Not applicable.

Consent to participate Not applicable.

Consent for publication Not applicable.

Competing interests The authors declare no competing interests.

References

1. Bijapur SD (2020) « Review on Advent of Additive Manufacturing », vol 8, nº 8
2. Kumar S (2010) « Selective laser sintering: Recent advances », in *Pacific International Conference on Applications of Lasers and Optics*, Wuhan, People's Republic of China: Laser Institute of America, p 607. https://doi.org/10.2351/1.5057211
3. Zhang J, Tan Y, Bao T, Xu Y, Xiao X, Jiang S (2020) Discrete element simulation of the effect of roller-spreading parameters on powder-bed density in additive manufacturing. Materials 13(10):2285. https://doi.org/10.3390/ma13102285
4. Chatham CA, Long TE, Williams CB (2019) A review of the process physics and material screening methods for polymer powder bed fusion additive manufacturing. Prog Polym Sci 93:68–95. https://doi.org/10.1016/j.progpolymsci.2019.03.003
5. Liu Y, Zhu L, Zhou L, Li Y (2019) Microstructure and mechanical properties of reinforced polyamide 12 composites prepared by laser additive manufacturing. RPJ 25(6):1127–1134. https://doi.org/10.1108/RPJ-08-2018-0220
6. Mousa AA (2014) « The Effects of Content and Surface Modification of Filler on the Mechanical Properties of Selective Laser Sintered Polyamide12 Composites », vol 8, nº 5
7. Tan P, Zhou M, Tang C, Zhou K (2024) A powder-scale multiphysics framework for powder bed fusion of fiber-reinforced polymer composites. Advanced Powder Materials 3(4):100190. https://doi.org/10.1016/j.apmate.2024.100190
8. Schmid M, Kleijnen R, Vetterli M, Wegener K (2017) Influence of the origin of polyamide 12 powder on the laser sintering process and laser sintered parts. Appl Sci 7(5):462. https://doi.org/10.3390/app7050462
9. Hofland EC, Baran I, Wismeijer etDA (2017) « Correlation of Process Parameters with Mechanical Properties of Laser Sintered PA12 Parts », *Advances in Materials Science and Engineering*, vol. pp. 1–11, 2017. https://doi.org/10.1155/2017/4953173
10. Karmiris-Obratański P, Papazoglou EL, Karkalos NE, Markopoulos AP (2024) Volume energy density and laser power: key determinants in SLS-processed PA12 mechanical properties. Int J Adv Manuf Technol 130(5–6):2505–2522. https://doi.org/10.1007/s00170-023-12806-y
11. Majewski C, Zarringhalam H, Hopkinson N (2008) Effect of the degree of particle melt on mechanical properties in selective laser-sintered Nylon-12 parts. Proc Inst Mech Eng B J Eng Manuf 222(9):1055–1064. https://doi.org/10.1243/09544054JEM1122
12. Salmoria GV, Hotza D, Klauss P, Kanis LA, Roesler CRM (2014) Manufacturing of porous polycaprolactone prepared with different particle sizes and infrared laser sintering conditions: microstructure and mechanical properties. Adv Mech Eng 6:640496. https://doi.org/10.1155/2014/640496
13. Stoia DI, Marşavina L, Linul E (2019) Correlations between process parameters and outcome properties of laser-sintered polyamide. Polymers 11(11):1850. https://doi.org/10.3390/polym11111850
14. Razaviye MK, Tafti RA, Khajehmohammadi M (2022) An investigation on mechanical properties of PA12 parts produced by a SLS 3D printer: an experimental approach. CIRP J Manuf Sci Technol 38:760–768. https://doi.org/10.1016/j.cirpj.2022.06.016
15. Wu J, Zheng J, Zhou H, Yang R (2019) Molten pool behavior and its mechanism during selective laser melting of polyamide 6 powder: single track simulation and experiments. Mater Res Express 6(8):085340. https://doi.org/10.1088/2053-1591/ab2747
16. Kozior T (2020) The influence of selected selective laser sintering technology process parameters on stress relaxation, mass of models, and their surface texture quality. 3D Printing and Additive

Manufacturing 7(3):126–138. https://doi.org/10.1089/3dp.2019.0036
17. Azam MU, Belyamani I, Schiffer A, Kumar S, Askar K (2024) Progress in selective laser sintering ofmultifunctional polymer composites for strain- and self-sensing applications. J Mater Res Technol 30:9625–9646. https://doi.org/10.1016/j.jmrt.2024.06.024
18. Chen P et al (2022) « Aging mechanism of polyetheretherketone powder during layer-wise infrared radiation of high-temperature laser powder bed fusion », *Materials & Design*, vol. 213, p. 110348, janv. https://doi.org/10.1016/j.matdes.2021.110348
19. Chen P et al (2020) Crystallization kinetics of polyetheretherketone during high temperature-selective laser sintering. Addit Manuf 36:101615. https://doi.org/10.1016/j.addma.2020.101615
20. Arai S, Tsunoda S, Yamaguchi A, Ougizawa T (2018) Effects of short-glass-fiber content on material and part properties of poly(butylene terephthalate) processed by selective laser sintering. Addit Manuf 21:683–693. https://doi.org/10.1016/j.addma.2018.04.019
21. Mokrane A, Boutaous M, Xin etS (2018) « Process of selective laser sintering of polymer powders: Modeling, simulation, and validation », *Comptes Rendus Mécanique*, vol 346, nº 11, Art nº 11, nov. https://doi.org/10.1016/j.crme.2018.08.002
22. Tang H, Chen H, Sun Q, Chen Z (2021) et W. Yan, « Experimental and computational analysis of structure-property relationship in carbon fiber reinforced polymer composites fabricated by selective laser sintering », *Composites Part B: Engineering*, vol 204, p. 108499, janv. https://doi.org/10.1016/j.compositesb.2020.108499
23. Morano C, Crocco MC, Formoso V, Pagnotta etL (2023) « Effect of induced plastic strain on the porosity of PA12 printed through selective laser sintering studied by X-ray computed micro-tomography », *Int J Adv Manuf Technol*, vol 125, nº 7–8, pp 3229–3240, avr. https://doi.org/10.1007/s00170-022-10791-2
24. Bourell DL, Watt TJ, Leigh DK, Fulcher B (2014) Performance limitations in polymer laser sintering. Phys Procedia 56:147–156. https://doi.org/10.1016/j.phpro.2014.08.157
25. Toth-Taşcău M, Raduta A, Stoia DI, Locovei C (2012) Influence of the energy density on the porosity of polyamide parts in SLS process. SSP 188:400–405. https://doi.org/10.4028/www.scientific.net/SSP.188.400
26. Magri AE, Bencaid SE, Vanaei HR, Vaudreuil S (2022) Effects of laser power and hatch orientation on final properties of PA12 parts produced by selective laser sintering. Polymers 14(17):3674. https://doi.org/10.3390/polym14173674
27. Zhu Z, Majewski C (2020) Understanding pore formation and the effect on mechanical properties of high speed sintered polyamide-12 parts: a focus on energy input. Materials Design 194:108937. https://doi.org/10.1016/j.matdes.2020.108937
28. « Rheological Properties of Polyamide PA 2200 in SLS Technology » (2020) https://doi.org/10.17559/TV-20190225122204
29. Olejarczyk M, Gruber P (sept. 2020) Ziółkowski, « capabilities and limitations of using desktop 3-D printers in the laser sintering process ». 10:6184. nº 18. https://doi.org/10.3390/app10186184
30. Jabri F-E, Ouballouch A, Lasri L, El Alaiji R (2025) Indirect effect of print surface bed temperature on surface roughness and dimensional accuracy of SLS polyamide 12 sintered parts. Int J Adv Manuf Technol. https://doi.org/10.1007/s00170-025-15995-w
31. Dooher T, Archer E, Walls T, McIlhagger A, Dixon D (2021) Ageing of laser sintered glass-filled polyamide 12 (PA12) parts at elevated temperature and humidity. Polym Polym Compos 29(9_suppl):S1294–S1304. https://doi.org/10.1177/0967391121 1027127
32. Morano C, Pagnotta L (2024) On powder bed fusion manufactured parts: porosity and its measurement. CMS 17(3):185–197. https://doi.org/10.2174/2666145416666230427093421
33. Abbott CS, Sperry M, et, Crane NB (oct. 2021) « relationships between porosity and mechanical properties of polyamide 12 parts produced using the laser sintering and multi-jet fusion powder bed fusion processes ». J Manuf Process 70:55–66. https://doi.org/10.1016/j.jmapro.2021.08.012
34. Lupone F, Tirillò J, Sarasini F, Badini C, Sergi C (2023) 3D printing of low-filled basalt PA12 and PP filaments for automotive components. J Compos Sci 7(9):367. https://doi.org/10.3390/jcs7090367
35. Shen F, Yuan S, Chua CK, Zhou K (2018) Development of process efficiency maps for selective laser sintering of polymeric composite powders: modeling and experimental testing. J Mater Process Technol 254:52–59. https://doi.org/10.1016/j.jmatprotec.2017.11.027
36. Singh S, Sharma VS, Sachdeva A, Sinha etSK (2013) « Optimization and Analysis of Mechanical Properties for Selective Laser Sintered Polyamide Parts », *Materials and Manufacturing Processes*, vol 28, nº 2, pp 163–172, févr. https://doi.org/10.1080/10426914.2012.677901
37. Singh S, Sachdeva A, Sharma etVS (2017) « Optimization of selective laser sintering process parameters to achieve the maximum density and hardness in polyamide parts », *Prog Addit Manuf*, vol 2, nº 1–2, pp 19–30, juin https://doi.org/10.1007/s40964-017-0020-4
38. Simha G, Martynková et al (2021) « Polyamide 12 Materials Study of Morpho-Structural Changes during Laser Sintering of 3D Printing », *Polymers*, vol 13, nº 5, p 810, mars., https://doi.org/10.3390/polym13050810
39. Wegner A, Witt G (2012) Correlation of process parameters and part properties in laser sintering using response surface modeling. Phys Procedia 39:480–490. https://doi.org/10.1016/j.phpro.2012.10.064